How Particle Size Influences Oxidation of Ancient Organic Matter during Weathering of Black Shale

Xin Gu* and Susan L. Brantley

Cite This: *ACS Earth Space Chem.* 2022, 6, 1443−1459

Read Online

ACCESS | Metrics & More | Article Recommendations | Supporting Information

ABSTRACT: Weathering continuously converts rock to regolith at Earth's surface while regulating the atmospheric concentrations of CO_2 and O_2. Shale weathering is of particular interest because shale, the most abundant rock type exposed on continents, stores much of the ancient organic carbon (OC_{petro}) buried in rocks. Using geochemical and mineralogical analysis combined with neutron scattering and imaging, we investigated the weathering profile of OC_{petro} in saprock in a black shale (Marcellus Formation) in the Ridge and Valley Appalachians in Pennsylvania, U.S.A. Consistent with the low erosion rate of the landscape, we discovered that Marcellus is completely depleted in carbonate, plagioclase, and pyrite in saprock below the soil layer. On the contrary, only ∼60% of OC_{petro} was depleted in saprock. By

comparing the pore structure of saprock to bedrock and samples combusted to remove organic matter (OM), we confirmed that the large particles of OM are preferentially depleted, leaving elongated pores of tens to hundreds of micrometers in length, while the smaller particulates of OM (ranging from ∼5 to ∼200 nm) are largely preserved during weathering. The retarded weathering of small OM particles is attributed to their close association with mineral surfaces in the shale matrix. The texture of OM in shale is underappreciated as an important factor that controls porosity generation and the weathering rate of OC_{petro}.

KEYWORDS: *black shale, organic matter, porosity, weathering, Marcellus shale, neutron scattering*
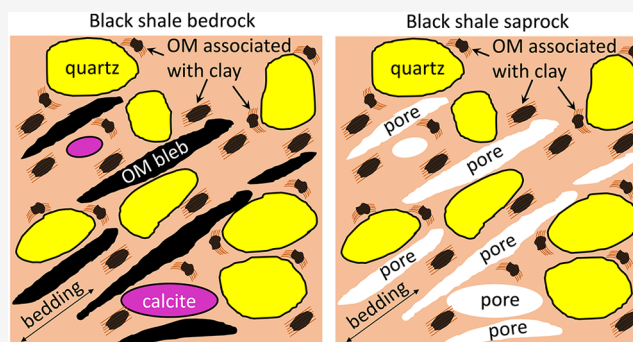
INTRODUCTION

Silicate weathering titrates acid gases released by volcanoes and, in particular, removes CO_2 from the atmosphere. At the same time, oxidative weathering of sulfide (mainly pyrite) and petrogenic organic carbon (OC_{petro}, also known as fossil, geogenic, or rock-derived organic carbon) consumes O_2[1] and releases CO_2.[2] In that respect, weathering is an important process in the control of the geological carbon and oxygen cycles.[3−5] However, the complexities of the O_2 and CO_2 cycles remain to be unraveled.[6] For example, a quantitative understanding of the interaction between oxidative weathering of pyrite and OC_{petro} and atmospheric pCO_2 and pO_2 requires a mechanistic understanding of the weathering process.[7,8]

To investigate the CO_2 and O_2 weathering cycles, shale is important because it covers 24−30% of the global land surface[9,10] and stores the majority of OC_{petro}.[11] Therefore, weathering profiles of OC_{petro} in shales have been analyzed[12−23] and modeled.[7] Depth profiles record the cumulative weathering process and can be deciphered to reveal mechanisms and rates of chemical reactions.[24,25]

As a result of these and other studies, the depletion of organic matter (OM) during black shale weathering has been attributed to various mechanisms, including (1) oxidation of OM to CO_2, (2) dissolution of OM to form dissolved OM,

and (3) loss by physical transport as particulate OM.[8] Furthermore, on the basis of observations of change in the amount and chemical composition of OM with depth, Petsch et al. argued that kerogen (the major component of OM in black shale) weathering is accomplished in two sequential steps, namely, non-selective oxidation + hydration, followed by cleavage + dissolution of the oxidized fragments. He further emphasized that the first step of oxidation is rate-limiting.[15] Consistent with oxidation as the rate-limiting step, Bolton et al. used a reactive transport code to model the oxidative weathering of OC_{petro}. In his model, oxygen is transported to OM at depth by diffusion of gaseous O_2 through the rock matrix.[7] The underlying assumption for this model is that delivery of the oxidant to the subsurface (when averaged over geological time scales) is a function of the erosion rate of the landscape, where erosion controls the rate of delivery of oxygen at depth. In this respect, oxidation of OM is like
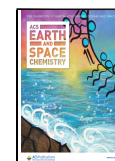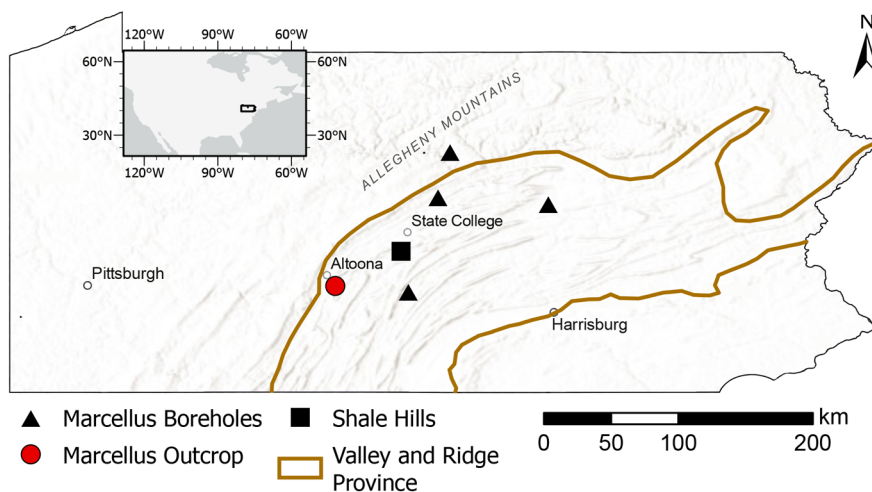
Figure 1. Map of study sites. Most sites are located within Valley and Ridge provinces in the Appalachians of Pennsylvania, U.S.A. The inset map shows the location of Pennsylvania in North America.

oxidation of pyrite, which has also been shown to be rate-limited by transport of oxygen and which, over geological time scales, is controlled by the erosion rate.[25,26] Indeed, in most studies of shale depth profiles, pyrite and OM have been observed to begin to oxidize at similar depths; however, the depletion profiles of pyrite and OM are usually decoupled at shallower depth.[15,17−19,21−23] For example, pyrite is completely depleted at the land surface in weathering shale, even up to some of the highest erosion rates observed globally today.[27] In contrast, complete depletion of OC_{petro} at the land surface is rarely observed in natural systems.[8] For example, in profiles developed on black shale in the northern Appalachian Basin, pyrite is already ∼100% weathered by ∼2 meters below land surface (mbls), but at that depth, only about 60−75% of the OC_{petro} has been lost, leaving a residual.[15] This retention of OC_{petro} occurs even though the shale is likely eroding at rates that are moderate to low, i.e., within the range of 0.012 ± 0.006 m $kyear^{-1}$ based on cosmogenic dating in the Appalachian region.[28] To our knowledge, no solutions to this puzzle have been proposed. We investigate this conundrum in this study by characterizing weathering profiles in saprock (weathered and fractured rock) of Marcellus shale (Middle Devonian-aged black shale) in a quarry in central Pennsylvania, U.S.A.

Retention of OC_{petro} at the land surface during weathering of a slow-eroding shale is particularly confusing because observations and reactive transport models of weathering black shale suggest that opening of porosity should be fast in the weathering rock, where acids generated by pyrite oxidation may enhance weathering rates.[20,29] In contrast to earlier studies that tended to focus on molecular changes in the OC_{petro},[12,13,15,30] we hypothesized that we could learn why some OM_{petro} is recalcitrant to weathering through analysis of the pore structure of the weathered and unweathered shale.

This study focuses on weathering of one member of the Marcellus Formation, a Middle Devonian unit dominated by shale that underlies approximately 70% of Pennsylvania (at depth) and much of West Virginia, as well as parts of Ohio, Maryland, and New York states in the U.S.A. This shale has been one of the major targets for shale gas development in the U.S.A.[31] Previous investigations of soil developed on exposed Marcellus in this region were focused on bulk soil and rock fragments in the upper 1.4 m and a few samples of subsurface

saprock with no focus on analysis of OC_{petro}.[20,32] Quantification of the loss of OC_{petro} is difficult as a result of the heterogeneous distribution of OC_{petro} in the bedrock of Marcellus. In this study, we investigated the weathering profile of Marcellus shale to a greater depth (∼11 m) and quantified the loss of OC_{petro} through analysis of the porosity profiles.

■ MATERIALS AND METHODS

Study Site. Saprock samples of Marcellus were collected from an outcrop at New Enterprise quarry (latitude, 40.4353°; longitude, −78.3421°) in Frankstown, PA, U.S.A. (Figure 1). The climate and erosion rate at the Frankstown site are similar to the rate measured nearby at the Shale Hills subcatchment of the Susquehanna Shale Hills Critical Zone Observatory (erosion rate, 0.01−0.025 m $kyear^{-1}$; mean annual precipitation, 107 cm; and mean annual temperature, 10 °C).[33] Both sites, 30 km apart from each other, are located in the Valley and Ridge provinces in the Appalachian Mountain region. The quarry exposes an outcrop in the lower Union Springs Member of the Middle Devonian Marcellus Formation.[34] This member is known to have some of the highest contents of total organic carbon (TOC) in the formation. The base of the unit is terminated by the underlying Onondaga limestone.[34]

The quarry was used to sample saprock, i.e., partially weathered and fractured but largely intact rock material. Given that the hillside of the quarry was excavated, leaving the outcrop under the ridgeline of the hill, we inferred that most of the weathering of the samples had occurred by downward weathering from the land surface prior to quarrying. A pickaxe was used to dig into the outcrop until resistance before samples were taken. Before sampling, ∼5 cm of easily disaggregated material at the surface of the outcrop wall was removed on the basis of methods previously described by Petsch et al.[15] The outcrop is mantled at the hilltop with a layer of soil of thickness of ∼0.3 m, but no soil was collected or studied because we assumed it would have suffered from human disturbance in the location. The shallowest samples are rock fragments collected from just below the soil−saprock interface at 0.3 mbls. The deepest oxidation was confirmed (as indicated by the extent of pyrite oxidation; see the Results and Discussion below) to terminate at the bottom of the shale saprock as delineated by the low-porosity and low-permeability

Onondaga Formation. This carbonate unit was dark gray in color and much harder to break compared to the overlying shale saprock.

Unweathered black shale from the same member and formation were also collected from drilled cores. Specifically, to estimate the geochemistry of the parent material (prior to weathering), 13 unweathered samples from the Union Springs Member were collected from four deep boreholes (>230 mbls) in central Pennsylvania (Figure 1 and Table S1 of the Supporting Information). Some analyses of these cores were summarized previously.[20,35,36] The boreholes were drilled and preserved by the Appalachian Basin Black Shales Group at The Pennsylvania State University. We emphasized weathering within the quarry profile only above the carbonate layer; therefore, we sampled putative parent shale in the deep cores by avoiding the carbonate-rich layers (layers with carbonate minerals of >50 wt %).

Geochemical, Mineralogical, and Microscopic Characterization. *Inductively Coupled Plasma Atomic Emission Spectroscopy (ICP−AES).* The air-dried rock fragments were pulverized using a mortar and pestle until they passed through a 100-mesh sieve (<150 μm). Major element chemistry of the pulverized aliquots was determined by ICP−AES (PerkinElmer Optima 5300DV ICP−AES) at the Laboratory for Isotopes and Metals in the Environment (LIME) at The Pennsylvania State University on solution after lithium metaborate fusion.[20] Loss on ignition (LOI) was determined by the difference in mass of sample before (nominally, 1 g) and after combustion at 900 °C for 1 h. All chemical analyses are presented on an as-received basis.

Mass Transfer Coefficient (τ). The elemental loss and gain during weathering was calculated as

$$\tau_{i,w} = \frac{C_{j,w} C_{i,p}}{C_{j,p} C_{i,w}} - 1 \tag{1}$$

where $\tau_{i,w}$ is the mass transfer coefficient of an element or mineral of interest[37,38] and $C_{j,w}$ and $C_{j,p}$ are the concentrations of an immobile element (i) or species of interest (j) in weathered material (w) or parent (p) (unweathered bedrock or protolith). The mass transfer coefficient can be used to quantify the elemental loss and gain if the parent material has been properly characterized and if element i is indeed immobile: when $\tau = 0$, element j is neither enriched nor depleted with respect to element j in the parent; when $\tau < 0$, the element has been lost relative to immobile element i in the parent; and when $\tau > 0$, the element has been added to the profile relative to the parent material.[37,38] To estimate parent composition here, we averaged the compositions of 13 unweathered samples from the Union Springs Member from the deep boreholes (Table S1 of the Supporting Information). We used Ti as the immobile element to describe the Marcellus shale because Ti (along with Zr) are the two least mobile elements during weathering in saprock in the Shale Hills subcatchment nearby.[39] Although Ti is somewhat more mobile than Zr in these soils, the concentration of Ti is ∼30 times higher than Zr in the parent of Marcellus and was therefore chosen as the immobile element to minimize errors incurred from analytical or parent variations.

Carbon and Sulfur. Total carbon and sulfur concentrations were determined on pulverized aliquots using a LECO SC632 carbon/sulfur determinator. Certified standards for total carbon and sulfur from National Institute of Standards and Technology (NIST) (NBS 2704) and United States Geological Survey (USGS) (SGR-1) were measured routinely to ascertain accuracy and precision. TOC concentrations were measured in several samples (acidified with 5% phosphoric acid) by the carbon/sulfur determinator following a United States Environmental Protection Agency (U.S. EPA) procedure (LG601).

X-ray Diffraction (XRD). Minerals were identified by XRD of the pulverized aliquots as described by Gu et al.[27] The relative mineral percentages were estimated semi-quantitatively using the USGS RockJock program.[40]

Scanning Electron Microscopy (SEM). To prepare sections for SEM, the rock fragments were cut perpendicular to bedding using a low-speed diamond saw, polished with sandpaper and diamond paste, and mounted on SEM stubs using carbon paste. A few samples were further polished by a broad ion beam milling system (Leica EM TIC 3X). The microscopy was performed on environmental SEM (FEI Quanta 250) or field-emission SEM (FEI Nova NanoSEM 630) as described by Gu et al.[27] Selected spots were probed by energy-dispersive X-ray spectroscopy (EDS) on SEM using an Oxford EDS detector. The XRD and SEM measurements were conducted at the Material Characterization Laboratory (MCL) of The Pennsylvania State University.

Selected grayscale backscattered electron (BSE) images (magnified between 60× and 300×) were segmented manually in ImageJ to create a binary image of mineral grain and pores.[41] The elongated pores, which were likely generated through decomposition and/or removal of OM (see the Discussion below), were selected and quantified using built-in Analyze Particles ImageJ plugin (size of >300 μm^2 and circularity between 0 and 0.2).

Mercury Intrusion Porosimetry (MIP). One saprock and one bedrock sample each were measured with MIP using a Micromeritics AutoPore V 9620 mercury porosimeter at pressures up to 413.7 MPa at MCL in The Pennsylvania State University using methods as described by Gu et al.[27] The pore throat size (r) was calculated from Washburn's equation

$$r = -4\gamma P^{-1} \cos \theta \tag{2}$$

where γ is the surface tension (0.485 N m^{-1} for mercury), θ is the contact angle (130° for mercury), and P is the applied pressure. With this analysis, mercury intrusion allows for measurement of pores with pore throats that range from 3 nm to 330 μm. The breakthrough capillary pressure, defined as the pressure at which a continuous connection of mercury develops through a porous medium, was determined from the inflection point of the convex-up sections of curves of cumulative mercury intrusion plotted versus mercury pressure.[42]

Neutron Scattering. The pore structure was characterized by a combination of neutron scattering and SEM imaging. Here, we only briefly introduce the theory and instrumentation, which has been thoroughly reviewed in the literature.[43,44] The scattering intensity, $I(Q)$, was measured as a function of modulus of the scattering vector Q, which is expressed as $Q = 4\pi\lambda^{-1} \sin \theta$, where λ is the wavelength of neutron and 2θ is the scattering angle.[43,44] The measured dimensions of scatters (e.g., pores) are in the range of ∼Q^{-1}. We used the pinhole small-angle neutron scattering (SANS) instrument [NGB30 beamline at National Institute of Standards and Technology Center for Neutron Research (NCNR)], which covers a Q range from 10^{-3} to 0.5 Å^{-1},[45] and the ultra-small-angle neutron

scattering (USANS) instrument (BT5 beamline at NCNR) using a double-perfect-crystal diffractometer that can measure a Q range from 10^{-5} to 10^{-3} Å^{-1}.[46] USANS and SANS measurements were conducted on thin sections of rocks with a thickness of 150−250 μm (the actual thicknesses were measured by a digital micrometer) under ambient conditions ("dry" measurements). Thin sections were saturated with a mixture of water (H_2O) and deuterated water (D_2O), which were designed to match the scattering length density (SLD) of the rock matrix. Because the variation of SLD of different minerals in Marcellus shale is smaller than the contrast of SLD between pores and the mineral matrix,[35] the measurements on thin sections after saturation with D_2O−H_2O ("wet, raw" measurements) were attributed to scattering from water-inaccessible pores. Measurements were also conducted on epoxy-impregnated (under vacuum) thin sections after saturation with D_2O−H_2O ("wet, epoxy-im" measurements) to distinguish pores that were impregnated with epoxy as epoxy-accessible pores (e.g., interconnected pores with large pore widths/throats or microfractures) and water-inaccessible pores. Given the reported values of the surface tension of typical liquid epoxy (0.015−0.042 N m^{-1})[47,48] and the contact angle between epoxy and mineral surface (25.5 ± 0.5°),[49] we estimated the minimum pore throat size to be 1 ± 0.5 μm during vacuum impregnation of epoxy (P = 1 atm) using eq 2. The contrast-matching approach has been previously applied to Marcellus shales from depth.[35,36,50]

(U)SANS data were normalized, reduced, and combined using a procedure available from NCNR.[51] For weathered Marcellus shale samples with pore dimensions larger than 10 μm, the (U)SANS data were further combined with BSE imaging data to extend the lower limit of Q to 10^{-7} Å^{-1} following the procedures described by Anovitz et al.[52] The scattering/imaging data were analyzed under the assumptions of the polydisperse spherical pore model to calculate the pore size distributions (PSDs, i.e., incremental porosity as a function of the pore size).[53] Because the actual pore geometries are far more complex than spherical, the pore dimensions reported here are approximations. However, a previous study has shown the overall trends of PSDs are similar among different models.[44] Therefore, because all of the scattering data were treated through the same procedure as in this study, we assume that the changes of PSDs among samples are robust indications of the change in the samples. The pore structure of weathered shale (usually with partially depleted OM; see the Results below) was compared to samples with 100% depleted OM after combustion at 450 °C for 16 h.[36] By doing this, we explored the change of texture of OM during weathering.

RESULTS

Parent Composition and Texture. A total of 13 samples from the Union Springs Member were averaged to determine a best estimate of the Marcellus parent in this location (Table 1 and Table S1 of the Supporting Information). Standard deviations for the average were used as an estimate of uncertainty in parent composition. XRD measurements and SEM images of selected parent samples indicated that illite and quartz are the two most abundant minerals in Marcellus, followed by chlorite, pyrite, carbonate minerals (calcite and dolomite), and plagioclase (Figure 2 and Table 2). In every potential parent sample analyzed, we observed at least 2 wt % carbonate minerals and 2.5 wt % plagioclase. The relatively low values of the carbonate content (2−10 wt %) are consistent

Table 1. Elemental Concentrations of Marcellus Shale Saprock Samples (the Deepest Sample PLG-14-3 Is from Onondaga Limestone) from the Outcrop at Frankstown, PA, U.S.A. (wt %, Except ppm for Zr, Reported on an As-Received Basis)

sample ID	depth (mbls)	Al[a]	Ca[a]	Fe[a]	K[a]	Mg[a]	Mn[a]	Na[a]	P[a]	Si[a]	Ti[a]	Zr[a]	LOI	C[b]	S[b]	TOC[c]
PLG-12-32	0.3	7.30	0.08	5.69	2.71	0.47	<0.01	0.04	0.03	28.4	0.43	115	10.8	4.40	0.054	4.40[d]
PLG-12-24	4.3	2.80	0.01	1.62	1.01	0.19	<0.01	0.04	0.03	35.2	0.14	47	13.5	8.87	0.178	8.87[d]
PLG-12-23	6.1	4.38	0.02	0.93	1.51	0.30	<0.01	0.05	0.01	33.3	0.23	80	14.4	9.01	0.289	9.01[d]
PLG-12-26	7.0	2.94	0.02	0.72	1.03	0.24	<0.01	0.04	0.02	35.7	0.14	64	14.1	10.6	0.164	10.6[d]
PLG-14-2	7.6	3.50	0.03	2.48	1.25	0.23	<0.01	0.05	0.07	34.9	0.19	59	11.6	6.32	0.368	6.32[d]
PLG-12-27	8.2	8.26	0.01	2.30	3.59	0.61	<0.01	0.06	0.04	29.4	0.44	133	12.2	6.31	0.293	6.31[d]
PLG-12-28	8.7	8.68	0.01	3.62	3.75	0.75	0.01	0.06	<0.01	28.7	0.49	141	10.4	3.41	1.907	3.41[d]
PLG-12-29	9.4	7.79	0.08	4.14	3.23	0.62	<0.01	0.06	<0.01	25.5	0.37	131	18.9	11.22	0.676	11.22[d]
PLG-14-3	10.9	1.15	32.62	0.87	0.53	0.55	0.10	0.04	0.03	4.6	0.06	17	37.6	11.14	0.482	2.13
parent[e]		7.66	2.20	4.49	2.61	0.87	0.02	0.52	0.04	26.7	0.42	119	11.87	4.55	2.46	3.6
		(1.32)	(1.23)	(0.80)	(0.51)	(0.19)	(0.01)	(0.14)	(0.01)	(2.0)	(0.08)	(32)	(2.92)	(2.30)	(1.52)	(1.9)

[a]Measured by ICP–AES. [b]Measured by the carbon/sulfur determinator after treating with hydrochloric acid (4 N) in these samples. [c]Measured by the carbon/sulfur determinator after acidification with phosphoric acid. [d]No effervescence was detected on treating with phosphoric acid; therefore, TOC was assumed to be the same as total carbon. [e]The parent concentrations are averages of samples from deep boreholes (n = 13; Table S1). The quoted uncertainties (in parentheses) are one standard deviation from the mean.
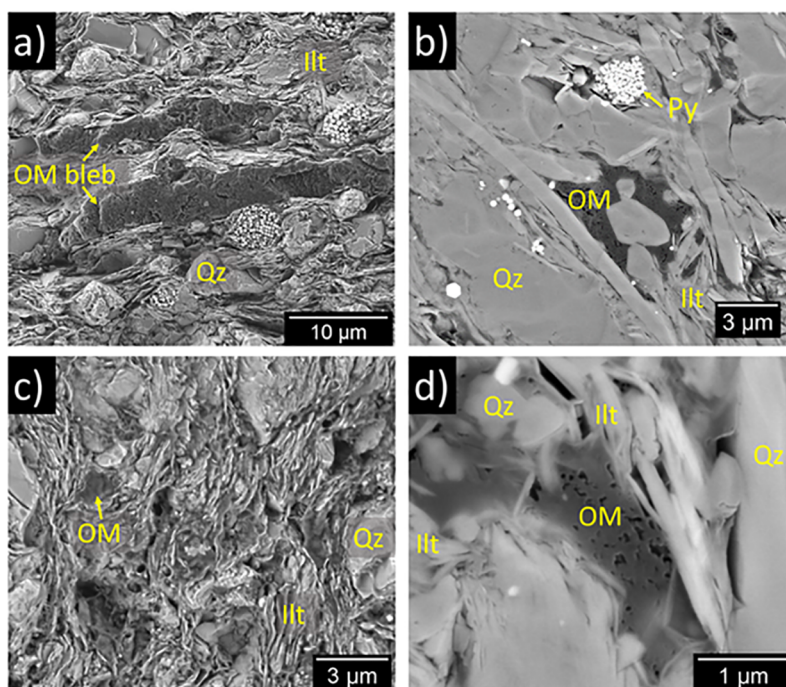
Figure 2. BSE images of unweathered bedrock of Marcellus shale (sample SS8721) from deep boreholes showing (a) big OM blebs (tens of micrometers in length) and (b−d) small OM particles (sub-micrometers to a few micrometers in size). The small OM particles are usually (b and d) located in pore space and/or (c and d) associated with clay minerals. Samples in panels b and d were polished through ion milling. Mineral codes are as follows: Ilt, illite; OM, organic matter; Py, pyrite; and Qz, quartz.

Table 2. Semi-quantitative Mineralogy for Marcellu Shale Samples (the Deepest Sample PLG-14-3 Is from Onondaga Limestone) from the Outcrop at Frankstown, PA, U.S.A.[a]

sample ID	depth (mbls)	Qz	Ill	Plag	Chl	Vrm	Carb	Kln	Fe oxides	Py	Jrs	other
PLG-12-32	0.3	47.4	34.6	1.3	ND[b]	4.0	ND	4.6	4.5	ND	ND	3.6
PLG-12-24	4.3	74.8	15.5	0.7	ND	2.9	ND	2.2	1.1	ND	1.0	1.8
PLG-14-2	7.6	72.6	14.2	1.5	ND	4.5	ND	0.9	1.5	ND	1.5	3.3
PLG-12-27	8.2	40.6	43.4	1.3	ND	3.0	ND	6.3	ND	ND	1.6	3.9
PLG-12-28	8.7	36.3	45.7	0.9	ND	3.3	ND	3.1	0.5	1.9	4.6	3.6
PLG-12-29	9.4	40.6	41.1	0.8	ND	1.2	ND	4.8	2.6	ND	5.4	3.5
PLG-14-3	10.9	5.9	5.6	ND	ND	ND	86.4	ND	0.5	1.4	ND	0.2
parent[c]		39.3 (6.7)	34.9 (4.2)	4.1 (1.5)	8.3 (3.4)	ND	6.1 (4.1)	ND	ND	4.4 (1.5)	ND	3.5

[a]Weight percent of minerals were determined by RockJock[40] and normalized to 100. Mineral codes are as follows: Qz, quartz; Ill, illite; Plag, plagioclase; Chl, chlorite; Vrm, vermiculite; Carb, carbonate (including calcite and dolomite); Kln, kaolinite; Py, pyrite; and Jrs, jarosite. [b]A concentration lower than 0.5 wt % was marked as not detected (ND). [c]The parent concentration was averaged through samples ($n = 6$) from deep boreholes reported by Gu et al.[35,36] The quoted uncertainty is one standard deviation from the mean.

with our sample plan to avoid high-carbonate layers in the deep Marcellus cores.

The abundance of sulfur and TOC in the Union Springs Member of Marcellus shale (sulfur, 2.5 ± 1.4 wt %; TOC, 4.2 ± 2.1 wt %) is similar to other black shales.[15] S-bearing minerals, such as barite and sphalerite, were only occasionally observed under SEM. Therefore, sulfur in the bedrock of Marcellus shale is almost entirely present in pyrite. We sometimes observed that the non-pyrite, S-bearing minerals were enriched in the Onondaga limestone at the base of the saprock and in carbonate-rich layers in the deep core of Marcellus as reported in the literature.[54,55]

Marcellus in this region experienced some degree of metamorphism during burial and exhumation during the Alleghenian orogeny and its aftermath. The OM in Marcellus shale in this region is therefore known to have relatively high maturity (as reflected by vitrinite reflectance R_0 values of

~2.2%).[35] The slight metamorphism also resulted in highly compacted textures: silt-sized grains, such as quartz, chlorite, pyrite, carbonate, OM, and plagioclase, are found as patches in a matrix dominated by illite (Figure 2). Consistent with the bulk composition measured by the carbon/sulfur determinator, OM particles and pyrite grains are frequently observed under microscopy in Marcellus. The dominant OM morphology observed at low magnification in Marcellus is elongated OM blebs parallel to the bedding and sometimes curved around rigid grains (Figure 2a). The sizes of such OM particles are usually tens of micrometers but can range up to hundreds of micrometers. At higher magnifications, we observed OM with amorphous shapes filling pore space (pores less than 1 μm in diameter) between rigid grains and OM associated with clay minerals (panels b−d of Figure 2). Single and aggregated euhedral pyrite crystals were commonly observed as framboids (panels a and b of Figure 2).

Saprock Profiles. In contrast to the deep core samples, no carbonates were detected by XRD in any of the Marcellus saprock from the outcrop at Frankstown quarry (Figure 3) and
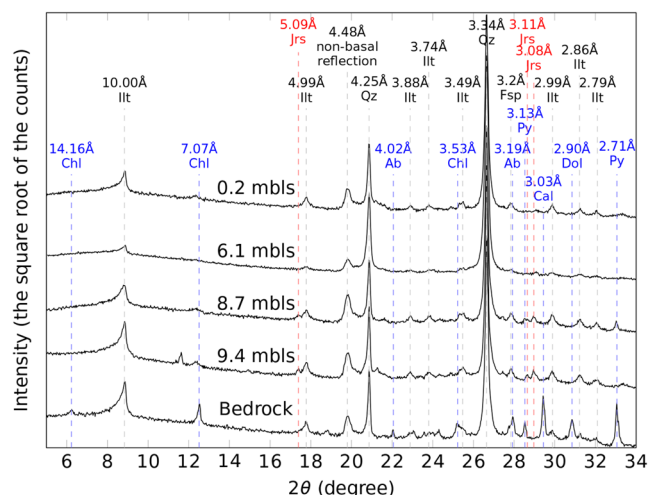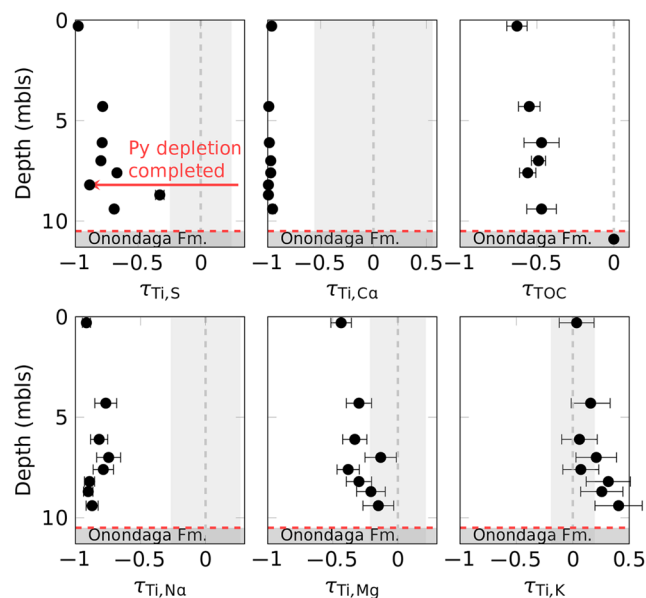

Figure 3. XRD patterns of saprock samples from the outcrop of Marcellus shale at Frankstown, PA, U.S.A. Numbers above peaks indicate the *d* spacing associated with that peak. The minerals in red were formed during weathering because they were not observed in bedrock, and the minerals in blue were transformed or depleted during weathering. The unweathered sample is from a deep borehole (sample SS8721 reported by Gu et al.[36]). Mineral codes are as follows: Ab, albite; Chl, chlorite; Fsp, K-feldspar; Ill, illite; Jrs, jarosite; and Qz, quartz.

no effervescence was observed when reacted with 4 N HCl. Similarly, plagioclase was always <1.5 wt % as determined by XRD. The mass transfer coefficients (τ) based on the average parent as described above (Table 1) for Ca and Na plotted versus depth therefore document depletion of the carbonates and plagioclase, respectively (Figure 4). Some of the variations in τ profiles may reflect the variation and stratigraphy of lithofacies across the profile (variability in parent material), as observed in other locations in the Appalachian basin.[56,57] However, the large depletion of Ca (>95%) and Na (>80%) across all profiles relative to the bedrock cannot be explained by the stratigraphic variations observed in the deep borehole samples (the gray area in Figure 4). In other words, we observed no parent material samples that totally lacked Ca and Na (carbonates and plagioclase). For these reasons, we attribute the depletion in Ca and Na to weathering.

With XRD, we similarly detected chlorite in every parent bedrock sample but detected no chlorite in the saprock samples (Table 2). We therefore inferred that chlorite was also weathered out of the saprock. Furthermore, weathering products of chlorite, such as vermiculite and kaolinite (which can also form from plagioclase weathering) and Fe oxides (which can also form from pyrite weathering), were only detected in the outcrop samples and never in the samples collected to represent parent materials (Figures 3 and 5 and Table 2). In contrast to carbonates, plagioclase, and chlorite, very little K was lost from the profile ($\tau_{Ti,K} \approx 0$). K is almost entirely present in the parent in illite (present at 35 ± 4 wt % estimated by XRD; Table 2).

In the bottom-most sample taken from Onondaga limestone, sulfide minerals (pyrite and sphalerite) were commonly observed (panels g−i of Figure 5) and no oxidation products


Figure 4. Elemental profiles of saprock samples from the outcrop of Marcellus shale at Frankstown, PA, U.S.A. (on the basis of elemental data in Table 1). The mass transfer coefficient (τ) was calculated through eq 1, using the average parent (Table S1 of the Supporting Information) and assuming that Ti is immobile. The τ values of TOC were estimated using eq 7. The vertical light gray bars around $\tau = 0$ reflect the variations of bedrock chemistry (Table S1 of the Supporting Information). The horizontal dashed red line indicates the onset of oxidation of pyrite. The horizontal red arrow indicates the completion depth of pyrite (∼8.2 mbls). Above this depth, pyrite was not detected by XRD and SEM−EDS.

of sulfide were detected by SEM−EDS. In the shale saprock, weathering products of pyrite, such as Fe oxide pseudomorphs (panels d−f of Figure 5), and precipitates of sulfate minerals, such as jarosite (panels a and b of Figure 5), were observed. These microscopic observations are consistent with partial depletion of pyrite and formation of sulfate minerals, as determined by XRD (Figure 4). At a depth of 8.2 mbls and at shallower depths, pyrite was not detected by either SEM−EDS or XRD. At the land surface, both pyrite and sulfate minerals are 100% depleted because $\tau_{Ti,S} \approx -1$ in the shallowest saprock sampled at 0.3 mbls.

Despite the clear depletion profiles of carbonate, sulfide, plagioclase, and chlorite compared to the deep core samples, the concentrations of TOC of all Marcellus saprock samples from the outcrop are close to or higher than the values of the bedrocks. This makes it difficult to quantify OM loss using eq 1. In the next section, we will summarize how we therefore used interpretation of porosity to quantify OM loss.

Porosity Profiles. We have previously shown that the contrast-matching experiments can be used in Marcellus shale to elucidate when pores are water-accessible.[35,36] For the unweathered bedrock samples recovered from deep boreholes, the scattering intensities of the "dry" measurements (blue dots in Figure 6) are only slightly higher than the "wet, raw" measurements (red dots in Figure 6). We also observed this for samples from the bottom-most Onondaga Formation of the outcrop. From this, we infer that most pores in these bedrock or carbonate-rich samples are water-inaccessible, because the contrast-matching fluids could not penetrate into the pores. In contrast, the scattering intensities of the "dry" measurements of the weathered shale (blue dots in Figure 6) are slightly higher
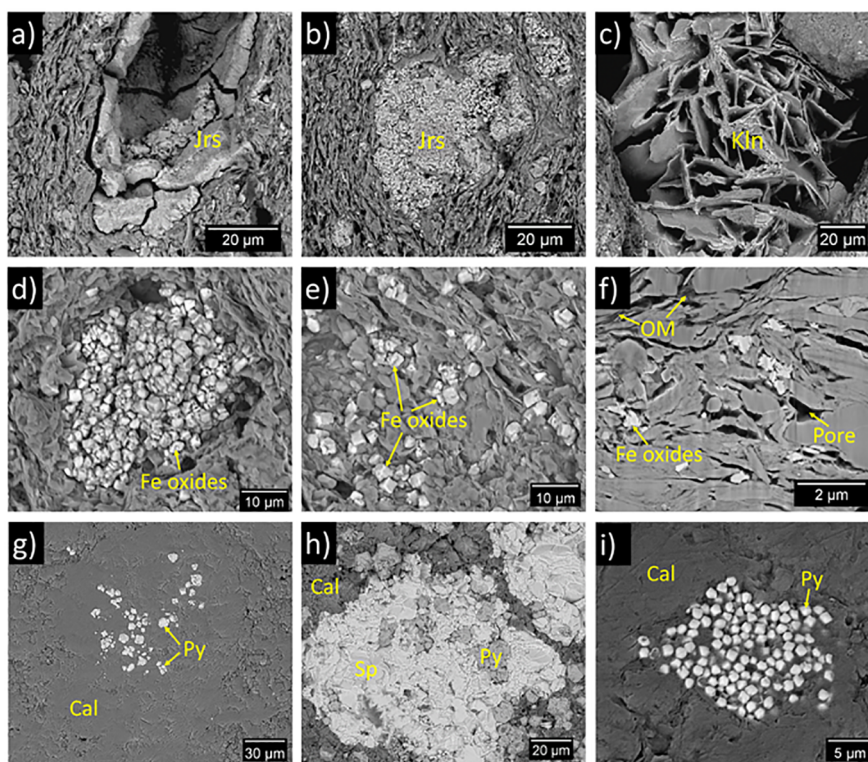
Figure 5. BSE images of samples from (a−f) saprock of Marcellus shale (8.7 mbls) and (g−i) underlying Onondaga limestone (10.9 mbls) from an outcrop at Frankstown, PA, U.S.A. Sulfide minerals (pyrite and sphalerite) are abundant, and no oxidation signatures were observed in Onondaga limestone. Secondary minerals, such as (a and b) jarosite, (c) kaolinite, and (d−f) Fe oxides pseudomorphs after pyrite (identified by SEM−EDS) were observed in the weathered shale. The sample in panel f was polished through ion milling. Mineral codes are as follows: Cal, calcite; Jrs, jarosite; Kln, kaolinite; OM, organic matter; Py, pyrite; Qz, quartz; and Sp, sphalerite.

than the "wet, epoxy-im" measurements (brown dots in Figure 6), and both are much higher than the "wet, raw" measurements (red dots in Figure 6). These results indicate that a large portion of the total porosity (total porosity inferred from "dry" measurements) is epoxy-accessible (inferred from "wet, epoxy-im" measurements) and a small portion of the total porosity is inaccessible to water (e.g., unconnected pores as inferred from "wet" measurements). The implication is that most widths or throats of pores in the shale saprock are larger than ∼1 μm and, therefore, can allow epoxy penetration.

More fine-structure information can be obtained through analysis of PSDs (right column of panels in Figure 6), as previously described in the literature.[27,42,43] For example, the sharp peak around 2 nm in the unweathered Marcellus shale reflects pores associated with clays (inter- and intracrystalline pores) as well as pores in OM.[35,36] Consistent with this, the Onondaga limestone sample with little clay and OM content does not exhibit the peak around 2 nm (Figure 6d) that is observed in other samples (panels b and f of Figure 6). The low porosity measured in the Onondaga limestone sample is consistent with the highly cemented (and undissolved) nature of the Onondaga limestone samples as observed under SEM (Figure 5g). In contrast, the Marcellus saprock samples exhibit a broad peak in the pore size range of micrometers to hundreds of micrometers in addition to the nanometer-sized peak associated with pores embedded among clays. In general, this broad peak is consistent with the size range documented by the peak for primary epoxy-accessible pores (brown, shadowed area in Figure 6b).
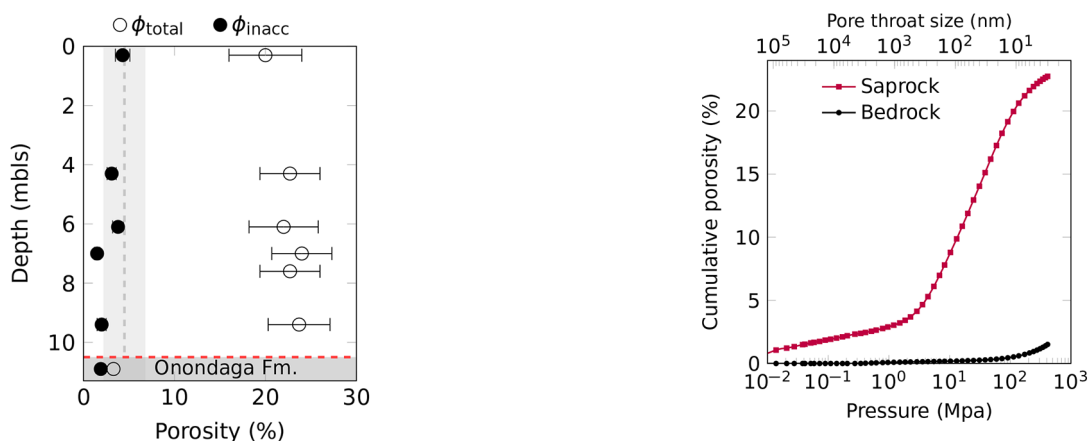
The total porosity values of all saprock samples from the outcrop of Marcellus shale at Frankstown, PA, U.S.A., measured by neutron scattering and imaging are more than 5-fold higher than the underlying Onondaga limestone and the bedrock of Marcellus (Figure 7). The water-inaccessible porosity values of the Marcellus saprock remain relatively constant with depth; therefore, most pores generated during weathering are water-accessible. Consistent with this, the bulk porosity of bedrock (3.7%, sample SS8721) measured by MIP is much lower than the value measured in saprock (22.7%, sample from 9.4 mbls). These porosity values are close to the values measured by neutron scattering and imaging. The breakthrough capillary pressure of saprock is 26 MPa, consistent with a critical pore throat size of 48 nm (Figure 8). For the bedrock sample, the breakthrough capillary pressure was not reached, indicating this critical pore throat size of <3 nm.

In saprock samples observed under SEM, pores were observed from micrometers to millimeters in dimension (Figure 9). The elongated pores are usually larger than tens of micrometers in length and are roughly oriented with the bedding (Figure 9a and Figures S1 and S2 of the Supporting Information), reflecting the same morphology as observed in the OM particles in bedrock (Figure 2a) and saprock samples (Figure S2 of the Supporting Information). Finer OM particles with amorphous shapes and that are associated with clays were also commonly observed in bedrock (panels b−d of Figure 2) and saprock samples (Figure 9d). The concentrations of carbon in the organoclay matrix ranges from 8 to 32 wt % (22 wt % on average) as determined by SEM−EDS on selected
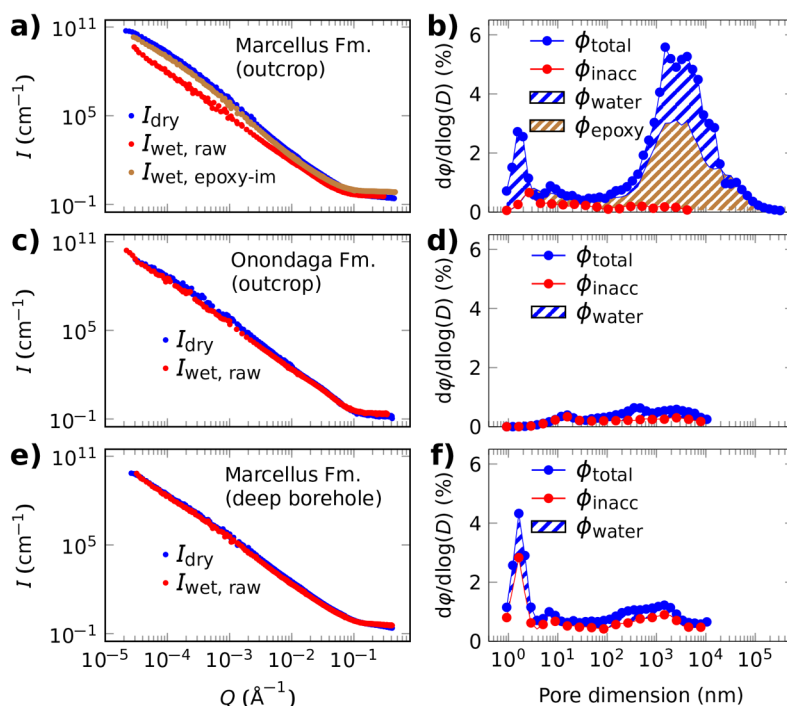
Figure 6. (Left column) Curves of neutron scattering and (right column) corresponding PSDs for (a and b) saprock of Marcellus shale (7 mbls) and (c and d) underlying Onondaga limestone (10.9 mbls) from an outcrop at Frankstown, PA, U.S.A. and (e and f) bedrock from a deep borehole (sample BE910 reported by Gu et al.[35]). The neutron scattering intensity (I) was plotted as a function of momentum transfer (Q), where the size of the scatterer is approximately equal to $2.5/Q$.[43] When $D_2O–H_2O$ of the same SLD as the shale enters pores, no scattering occurs. Therefore, the difference between scattering intensities of "dry" measurement and "wet, raw" measurement reflects the water-inaccessible porosity (ϕ_{inacc}), and the difference between scattering intensities of "wet, epoxy-im" measurement and "wet, raw" measurement reflects the epoxy-accessible porosity (ϕ_{epoxy}). The curves of PSDs derived from neutron scattering data lined up with the appropriate panels on the left. For the (b) saprock of Marcellus shale, the porosity was calculated by scattering + imaging data.
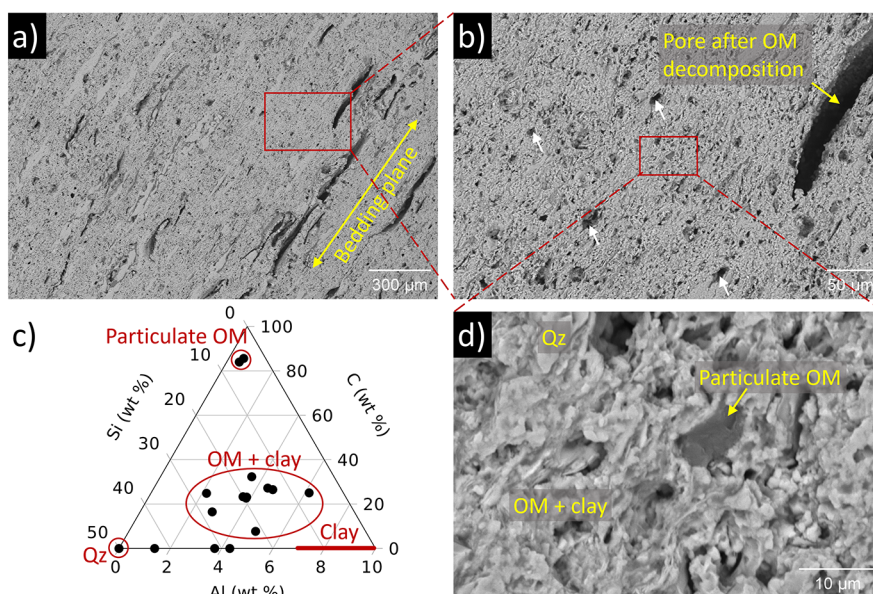

Figure 7. Porosity profiles of saprock samples from the outcrop of Marcellus shale at Frankstown, PA, U.S.A. The total porosity (ϕ_{total}) was calculated through neutron scattering and imaging data ("dry" measurements), and the inaccessible porosity (ϕ_{inacc}) was measured on samples after contrast-matching through neutron scattering ("wet" measurements) as described in the text. The vertical light gray bars reflect the variations of total porosity of bedrock (Table S1 of the Supporting Information). The horizontal, dashed, red line indicates the onset of oxidation of pyrite.


Figure 8. Cumulative porosity as a function of the mercury injection pressure for Marcellus shale bedrock from deep borehole (sample SS8721 reported by Gu et al.[36]) and saprock from an outcrop at Frankstown, PA, U.S.A. (9.4 mbls).

through dissolution of carbonate grains were also observed (e.g., pores marked by white arrows in Figure 9b).

The textural changes of OM during weathering were further explored by comparing the curves of PSDs of weathered samples from different depths (top row of panels in Figure 10), in which OM is partially depleted, to samples with different initial TOC values (bottom row of panels in Figure 10), in which OM was completely removed by combustion.[36] In comparison to the weathered samples, the combusted samples have a higher fraction of pores within the range from ~5 to

spots (areas varied from 20 to 100 μm^2) on a saprock sample (7.0 mbls; Figure 9c and Figures S1 and S3 of the Supporting Information). Some equant pores (usually smaller than tens of micrometers in size) that look like they may have formed

Figure 9. (a, b, and d) BSE images of a saprock sample from an outcrop of Marcellus shale at Frankstown, PA, U.S.A. (7.0 mbls) show the generation of porosity at different scales. The elongated pores (tens to hundreds of micrometers in length) oriented with the bedding were likely to be generated through OM decomposition. The white arrows in panel b indicate equant pores with micrometers to tens of micrometers in size, which were likely to be generated through dissolution of carbonates. (d) OM associated with clay was commonly observed at micrometer scales, as indicated by (c) ternary plot of elemental composition of selected spots determined by SEM−EDS (raw data in the Supporting Information). Mineral codes are as follows: OM, organic matter; Qz, quartz.
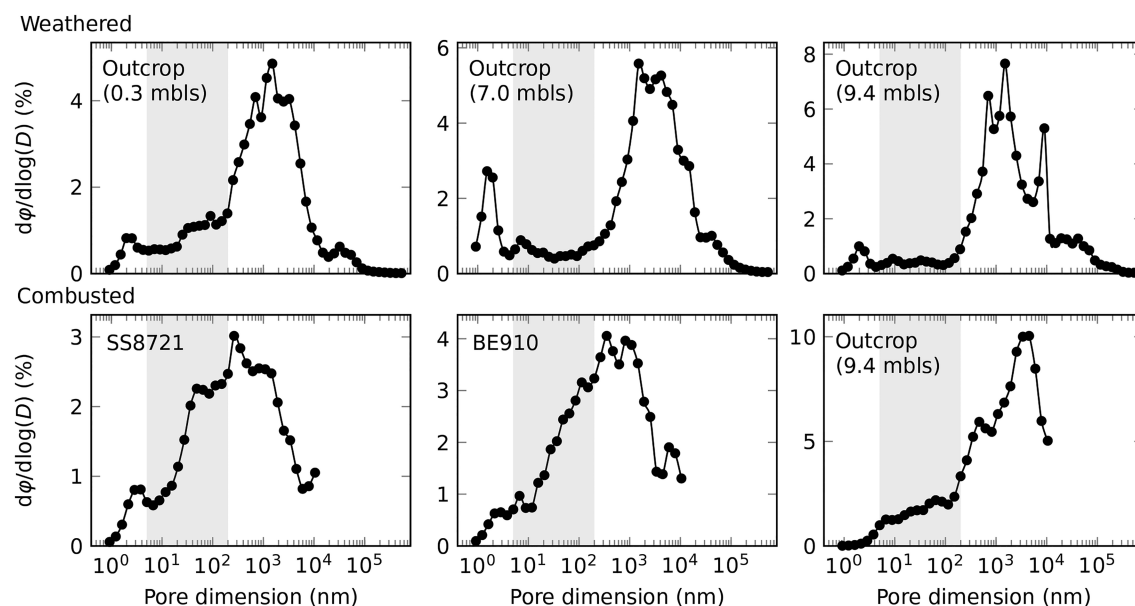
Figure 10. Curves of PSDs of Marcellus saprock samples collected from (top row of panels) outcrop at Frankstown, PA, U.S.A. and (bottom row of panels) combusted samples. The curves of PSDs of saprock samples were calculated from neutron scattering and imaging data, and those of combusted samples were calculated from neutron scattering data only, because the images are not available. Samples SS8721 and BE910 are bedrock samples from deep boreholes, and the results were published by Gu et al.[36]

~200 nm (highlighted by the gray bar in Figure 10). The implication from these observations is that combustion removed both small and large OM particles, while weathering preferentially removed large OM particles (>200 nm).

◼ DISCUSSION

Reaction Fronts for S- and Ca-Containing Minerals and Acid Generation. The τ plots for S and Ca indicate depletion profiles of S- and Ca-containing minerals in the

saprock of Marcellus shale (Figure 4); however, the depths of the reaction fronts are different. Carbonate minerals were completely depleted in saprock of Marcellus shale, as evidenced by >95% depletion of Ca (Figure 4), XRD measurements (Figure 3), and the HCl effervescence test. Therefore, the sharp reaction front (τ value changes from 0 to −1 in a small depth interval) of carbonates is located at the lithological contact between Marcellus shale and the underlying Onondaga limestone at ~10.7 mbls. On the contrary,

pyrite was detected by both XRD and SEM−EDS in saprock of Marcellus from 8.2 to 9.4 mbls. Noting that no oxidation signature was observed in the underlying Onondaga limestone, we suspect that pyrite oxidation initiated at the bottom of Marcellus ($\sim$ 10.7 mbls) and reached approximately 100% completion at 8.2 mbls. However, the τ value of S does not drop to −1 at this depth (Figure 4) as a result of the formation of jarosite detected by XRD and SEM−EDS (Figures 3 and 5). A trace amount of S (up to 0.2 wt %) may present in OC_{petro} based on the concentration of S in OM determined by SEM−EDS (0.9−1.7 wt %; Figures S1−S3 of the Supporting Information). At the base of the soil (our uppermost samples), both pyrite and jarosite are completely removed, as indicated by >95% depletion of S.

The deeper depletion depth of carbonate than pyrite might be related to the downward infiltration of acidic water generated through pyrite oxidation.[58] The pyrite oxidation reaction generates 4 mol of protons (H^+) per mole of pyrite (eq 3).

$$4FeS_2(s) + 15O_2(aq) + 14H_2O$$
$$\rightarrow 8SO_4^{2-}(aq) + 16H^+(aq) + 4Fe(OH)_3(s) \qquad (3)$$
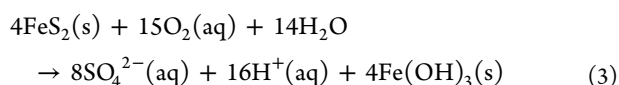
If carbonate minerals are present in high enough abundance, H^+ is consumed through carbonate dissolution *in situ*, but if the carbonate is not sufficient, excess H^+ may infiltrate downward to dissolve carbonate beneath. The acid balance can be calculated from the acid-generating capacity R of the rock (modified from Brantley et al.[59])

$$R = 4M_{pyrite} - M_{IC} \qquad (4)$$

where M_{pyrite} and M_{IC} are the molar concentrations of pyrite and inorganic carbon (IC) in bedrock, respectively. When R values are smaller than 0, oxidation of pyrite only affects the extent of carbonate dissolution at the same depth and the reaction front of carbonate is the same or shallower than pyrite; when R is larger than 0, excess H^+ will generate a dissolved zone beneath the reaction front of pyrite. Using data in Table S1 of the Supporting Information, the R value of Marcellus shale is 1.54 ± 0.72 mol kg^{-1}, consistent with the likelihood of a deeper reaction front for carbonate than pyrite, as observed in the outcrop of Marcellus shale.

The high acid-generating capacity in Marcellus is also consistent with the secondary minerals that form after pyrite oxidation. In contrast to previous observations on weathering of a nearby pyrite-poor shale, where jarosite was never detected (the Rose Hill),[25] we not only observed Fe oxide pseudomorphs (*in situ* products of pyrite oxidation) but also observed jarosite (as an *ex situ* product of pyrite oxidation) precipitated in pore space. Jarosites, known to form at low pH, often require low pH to remain stable (e.g., pH < 3.5).[60−62]

High values of acid-generating capacity are likely necessary to form jarosite during weathering because (1) the solution pH must remain low and (2) the acidity enhances the dissolution of silicates to provide cations (e.g., Na^+ and K^+) and pore space for jarosite formation. For example, jarosite in abundances of up to 10 wt % (as determined by XRD) was observed in New Albany shale saprock in Kentucky.[19] On the basis of the total sulfur (2.7 wt %) and Ca (0.86 wt %) concentrations of one of the New Albany cores,[19] we calculated the R value as 1.47 mol kg^{-1} (allocating all S to pyrite and all Ca to calcite), i.e., similar to the R value calculated here for Marcellus. Also, the completion depth of pyrite oxidation (8.1 mbls) is shallower

than the completion depth of carbonate dissolution (12.8 mbls) in the outcrop of New Albany shale, consistent with our observation at the Marcellus outcrop. In contrast, jarosite was never observed in saprock samples of Mancos shale in Colorado, where we calculated a R value of −0.48 ± 0.52 mol kg^{-1}.[22] This value is based on the total sulfur (1.1 ± 0.5 wt %) and IC (1.4 ± 0.5 wt %) concentrations of parent Mancos reported by Wan et al.[22] and the assumption that all S can be attributed to pyrite. On the basis of observations from four boreholes in the study site of Mancos shale, pyrite oxidation always completes deeper or at the same depth compared to carbonates.[22] The inference is that all acidity generated through pyrite oxidation in Mancos is buffered by carbonate and that R is a useful indicator of these relative depths of reaction.

Estimating TOC Depletion. One of the most difficult tasks in characterizing weathering is to define the parent composition. Given that the TOC in the Marcellus shale varies significantly with locality and depth,[31,57] we collected samples from carbonate-poor strata in the deep boreholes in the Union Springs Member of Marcellus and averaged those to estimate parent compositions (Table S1 of the Supporting Information). However, we noticed that, in the weathered saprock samples, TOC contents were larger than this average value, even though we saw ample evidence under SEM for OM depletion (Figure 9a and Figures S1 and S2 of the Supporting Information). The high TOC contents in the saprock would not likely come from modern OM on the surface because (1) modern OM is usually enriched in soils but not enriched in the saprolite or saprock underneath,[63] and (2) if the modern OM plays an important role in the OC pool of the saprocks, we could imagine the shallowest saprock sample to have the highest TOC. However, we observed the opposite: the shallowest saprock has the lowest measured TOC (Figure 11). The retention of TOC in saprock suggested the possibility
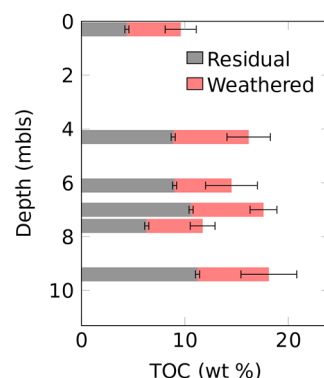
Figure 11. Weathering profile of TOC for weathered Marcellus shale. The content of weathered TOC was calculated using eq 6 based on values of ϕ_{OM} calculated through image segmentation.

that the TOC was weathering, but the rate was not as fast as other minerals, such as pyrite and carbonate. We therefore used the porosity in samples to infer the original TOC concentrations in the no longer present parent as well as the extent of weathering of TOC for depth intervals in the profile. In this approach, we assumed that the elongated, large pores observed in the SEM images of weathered Marcellus (panels a and b of Figure 9) were generated through OM decomposition

Table 3. Summary of Pore Structure Characteristics for Marcellus Shale Samples (the Deepest Sample PLG-14-3 Is from Onondaga Limestone) from the Outcrop at Frankstown, PA, U.S.A.[a]

sample ID	depth (mbls)	ϕ_{total} (%)	ϕ_{inacc} (%)	ϕ_{epoxy} (%)	ϕ_{water} (%)	ρ_b (g cm^{-3})[b]	ρ_s (g cm^{-3})[c]	ϕ_{OM} (%)[d]	ϕ_{OM} (%)[e]	TOC$_{weathered}$ (wt %)[f]	TOC$_{weathered}$ (wt %)[g]
PLG-12-32	0.3	20.0 (4.0)	4.3 (0.8)	8.5 (2.5)	7.2	NM[h]	NM	7.6 (2.2)	8.5 (5.6)	5.2 (1.5)	5.9 (3.8)
PLG-12-24	4.3	22.7 (3.3)	3.1 (0.5)	NM	NM	NM	NM	10.7 (3.0)	11.2 (5.1)	7.3 (2.1)	7.7 (3.5)
PLG-12-23	6.1	22.0 (3.8)	3.8 (0.6)	NM	NM	NM	NM	8.1 (3.7)	10.5 (5.5)	5.5 (2.5)	7.2 (3.7)
PLG-12-26	7.0	24.0 (3.3)	1.5 (0.3)	11.4 (2.8)	7.1	NM	NM	10.3 (1.9)	12.5 (5.1)	7.0 (1.3)	8.6 (3.5)
PLG-14-2	7.6	22.7 (3.3)	NM	NM	NM	NM	NM	8.0 (1.7)	11.2 (5.1)	5.4 (1.2)	7.7 (3.5)
PLG-12-29	9.4	23.7 (3.4)	2 (0.5)	10.4 (2.5)	11.3	1.990	2.576	10.1 (3.9)	12.2 (5.2)	6.9 (2.7)	8.5 (3.5)
PLG-14-3	10.9	3.3 (0.8)	1.9 (0.5)	NM	NM	NM	NM	NM	NM		
parent		5.8 (2.5)				2.433	2.470				

[a]The porosities were derived from a combination of neutron scattering and BSE imaging data using the polydisperse sphere model as described in the text. The quoted uncertainty is one standard deviation from the mean. [b]Bulk density measured by the mercury porosimeter. [c]Skeletal density (density of solid mineral grains, excluding pores accessible to mercury at the highest applied pressure) measured by the mercury porosimeter. [d]The porosity that was attributed to decomposition of OM and calculated from image segmentation. The uncertainties were calculated as the standard deviation of results obtained for different images on the same sample. [e]Calculated through porosity allocation using eq 5. The uncertainties were calculated by propagation of uncertainties of ϕ_t, ϕ_b, and V_{carb}. [f]Weathered TOC content in saprock calculated using eq 6 on the basis of ϕ_{OM} estimated from image segmentation through porosity allocation. [g]Weathered TOC content in saprock determined on the basis of ϕ_{OM} estimated through porosity allocation. [h]NM = not measured.

(ϕ_{OM}). We quantified ϕ_{OM} through image segmentation using ImageJ (Table 3).

In another approach, we quantified ϕ_{OM} through porosity allocation. To do this, we assumed that volume is neither generated nor lost during weathering of pyrite, plagioclase, and chlorite at least in the saprock samples studied here. This assumption is defensible because pyrite oxidation, plagioclase to kaolinite transformation, and chlorite to vermiculite/kaolinite transformation are usually assumed to be pseudomorphic. In addition, loss of the secondary minerals (Fe oxides, kaolinite, and vermiculite) appears negligible because summations of values of secondary mineral volumetric abundances roughly equal the loss of primary minerals. With this set of assumptions, ϕ_{OM} was calculated as the difference between the total porosity of weathered Marcellus measured by neutron scattering and imaging (ϕ_t) and the summation of the porosity of bedrock (ϕ_b = 5.8 ± 2.5%; Table 3) and the volume fraction of carbonate measured in the bedrock (V_{carb} = 5.7 ± 3.2%, estimated from the mineral abundance values in Table 2; carbonate was assumed to be completely depleted in saprock).

$$\phi_{OM} = \phi_t - V_{carb} - \phi_b \tag{5}$$

The values of ϕ_{OM} estimated through porosity allocation using eq 5 are consistent with those derived directly from image segmentation (Table 3). The fraction of TOC content that is weathered (mass of weathered TOC/mass of saprock, wt %) was then calculated as

$$TOC_{weathered} = \frac{\phi_{OM}\rho_{OM}\beta}{\rho_{saprock}} \tag{6}$$

where ρ_{OM} is the density of OM (1.6 g cm^{-3} as measured in Marcellus shale),[36] β is the mass fraction of C in OM (0.85, on the basis of the stoichiometry of OM in the Marcellus shale, $C_{10}H_5O$),[35] and $\rho_{saprock}$ is the bulk density of saprock of Marcellus shale (2 g cm^{-3}; Table 3). Assuming weathering of saprock of Marcellus is isovolumetric, we can calculate the mass transfer coefficient of TOC (τ_{TOC}) as

$$\tau_{TOC} = -\frac{TOC_{weathered}}{TOC_{weathered} + TOC_{residual}} \tag{7}$$

where TOC$_{residual}$ is the TOC value measured in saprock and TOC$_{weathered}$ + TOC$_{residual}$ is the original TOC value in saprock. The results indicate that the original TOC content is 8−18 wt %, and 47−63% of it was lost during weathering (Figure 11). The reconstructed TOC values are consistent with the high TOC values (Table 3) observed in the basal Union Springs Member as reported in the literature[31] and are close to the upper bound of reported TOC values of Marcellus.[57]

Interpretation of the Incomplete Reaction Front of OC$_{petro}$. In contrast to the complete depletion of carbonate and pyrite at the land surface, the τ plot for TOC indicates that about 45% of the TOC is lost in the first half meter of weathering, but this fraction remains relatively constant or increases to only 63% at the shallowest saprock (Figure 4). Using the nomenclature by Brantley and White,[64] the profile for TOC is incompletely developed because it shows partial depletion, even at the land surface. This result for weathered Marcellus shale is consistent with depletions reported for the same shale exposed to weathering at Huntingdon, PA, U.S.A. (τ_{TOC} of the shallowest saprock ≈ −0.5),[20] and Herkimer, NY, U.S.A. (τ_{TOC} at land surface ≈ −0.6).[15] In fact, of the 16 locations where depletion of OM in saprock has been reported (for a total of 11 sedimentary rocks), incompletely developed profiles of weathering were reported in 10 sedimentary rocks and 13 locations. Weathering of OM to near completion (τ_{TOC} < −0.95) was reported in only three locations, one each on New Albany,[17] Woodford,[15] and Green River.[15]

Several factors can explain such incomplete development with respect to any component X in eroding systems:[24] (i) atmospheric additions or biopumping adds X to topsoil; (ii) as X degrades, a new form of more recalcitrant X reprecipitates; (iii) X is present in multiple forms such that some decomposes or dissolves, while some is more recalcitrant to decomposition or dissolution; and (iv) the time scale required to weather all of the X is long compared to the residence time of particles in the zone of weathering (=weathering zone thickness/rate of erosion). Explanations i and ii are unlikely because we have not found evidence in the literature for OC$_{petro}$ in dust or for enrichment of OC$_{petro}$ during biocycling. Instead, the observation that much of the OC$_{petro}$ decomposes rapidly and the rest remains throughout the profile suggests that both explanations iii and iv are true. In other words, about half of
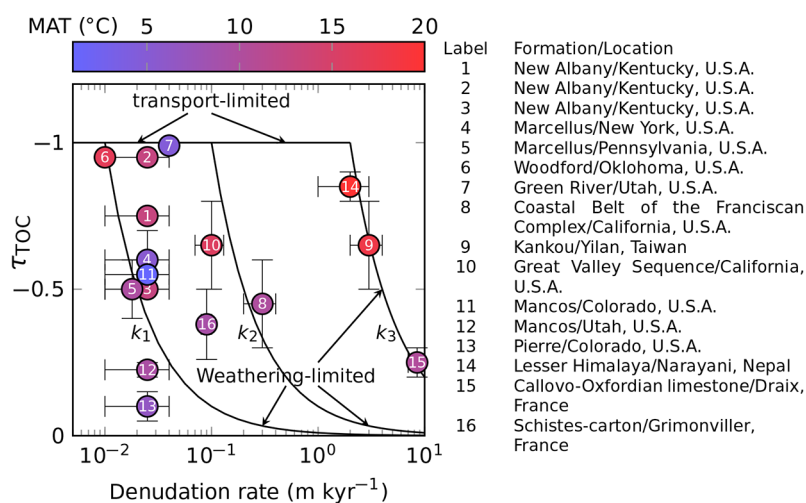
Figure 12. Mass transfer coefficient for TOC (τ_{TOC}) for the shallowest saprock sample as a function of the estimated denudation rate. The curves were calculated as in Figure 8b by Lebedeva and Brantley.[77] In the regions with a low denudation rate, the rate of supply of unaltered rock to surficial conditions by erosion (denudation rate) is slower than the weathering rate (the rate constants $k_3 > k_2 > k_1$) and TOC is completely depleted near the land surface ($\tau_{TOC} = -1$). In the regions with high denudation rate (e.g., higher than the weathering rate), TOC is incompletely depleted near the land surface ($\tau_{TOC} > -1$). The points show values estimated in small watersheds developed on sedimentary rocks, and the error bars represent two standard deviations (Table S2 of the Supporting Information). The color of the points represents MAT of each watershed. See Table S2 of the Supporting Information for the details of each site. Shales in warmer climates tend to show higher extents of depletion of TOC.

the OC_{petro} is rapidly decomposed and half is so recalcitrant that it remains almost to the land surface.

One reason that some of the OC_{petro} might be very refractory is that it could contain more (bio)chemically unreactive compounds that resist oxidation. For example, Loucks and Reed proposed that OM filled-in intraparticle pores in black shales can originate from migrated bitumen or oil, which is chemically different from depositional OM.[65] We cannot refute this possibility because we made no assessments of the nature of the OM in the samples and whether degradation of OM in shale during weathering is selective has not been established in the literature. For example, Petsch et al. studied the compositional change of OM in several black shale weathering profiles through solid-state ^{13}C nuclear magnetic resonance (NMR) and found that OM loss is selective in some shales (e.g., aliphatic C was more depleted than aromatic C in Woodford shale) but non-selective in others (e.g., highly aliphatic Green River shale).[30] In addition, an investigation on a global data set of OC bond-strength diversity indicates that OM degradation in soils/sediments is non-selective as a result of the interactions with the mineral matrix.[66] Here, on the basis of the microscopic observations and neutron scattering measurements, we propose an alternate or additional explanation that could occur regardless of possible compositional factors. Specifically, almost all of the large OM particles (0.2−200 μm) with elongated shapes are depleted completely in the saprock. In contrast, small grains of OM (5−200 nm) disseminating throughout the mineral matrix away from the large OM particles appear to remain in the saprock, as evidenced by the images (Figure 9d) and the composition of the organoclay matrix (8−32 wt % C; Figure 9c). Only near the land surface above 7 mbls, we see a gradual increase in the fractions of pores in the range from around 5 to 200 nm that could be attributed to depletion of the finer OM (Figure 10). If this is the explanation for the τ_{TOC} plot behavior, this might imply either that the large particles are lost by a mechanism

that does not work on small particles or that the OM in the small particles contains more refractory components.

Weathering Mechanism of OC_{petro}: The Role of the Particle Size. One possibility to explain preferential loss of large OM particles would be plucking and subsurface transport of the particles and removal in groundwater. However, such subsurface particle transport has been observed in shales to be restricted to clay-sized (i.e., micrometer or sub-micrometer) particles.[39,67] Furthermore, although it does not occur in all profiles studied in the literature, Petsch et al. have shown that the oxygen.carbon ratios in OM increase as the OM depletes in most shale weathering profiles, leading to the inference that oxidative dissolution is the dominant mechanism of depletion.[15] Oxidative degradation of OM in black shale, especially OM particles with elongated shape, was observed after reacting with strong oxidizers (ammonium persulfate and sodium bromate) in a laboratory experiment.[68] Oxidation as the mechanism is also consistent with the observation that both pyrite and OM decomposition initiates at similar depths in Marcellus studied here (Figure 4) as well as in the many other profiles of black shale weathering.[14,15,17,19,22,23] Such oxidation may be biotically mediated because some bacteria and fungi have the capability to use OC_{petro} as carbon and energy sources.[63,69,70]

Assuming that oxidation is the mechanism for loss of large particles, we are left with the puzzle of why the smaller particles oxidize less rapidly. For example, it has been shown that microorganisms cannot access pyrite, a well-known substrate for microbially catalyzed oxidation reactions, in the shale matrix at depth because of the small pore throats of shale.[25] This argument rests upon the observation that the smallest microorganisms in groundwater that have been reported are ~100 nm in size.[71] In the saprock of Marcellus, the small critical pore throat size (48 nm) is also likely to physically limit the access of microorganisms into the smaller OM particles embedded in the shale matrix. However, the importance of microbial activity in controlling the weathering

flux of OC_{petro} remains debatable.[8] Nonetheless, small pore throats could also affect the diffusivity of oxidants,[25,50] lowering the rate of abiotic oxidation of OM as well. After decomposition of large OM particles, additional pore throats become large enough (>1 μm) to allow for epoxy penetration, and these are likely large enough pathways for microbial access and fast diffusion of the oxidant. Thus, the large OM particles are probably more accessible to oxidants and perhaps to microorganisms than the small OM particles embedded in the shale matrix.

Another possibility for faster decomposition of larger particles is the association of small particulate OM with clay. The size of the smaller OM particles (∼5−200 nm) is consistent with the size of modern OM particles observed in many soils and sediments,[72,73] and such particles are usually associated with clay minerals. The clay association inhibits oxidation of modern OM in marine sediments[74] and in soil.[66,75,76] The clay minerals may physically limit the access of oxidants and microorganisms as discussed above and/or chemically stabilize OM by forming bonds with the mineral surface.[66] Either mechanism could explain the preferential preservation of clay-associated OM in black shales, and our observation could not exclude one from the other. In his early study, Bolton et al. discounted the association of OM with mineral surfaces as a possibility for inhibition of oxidative weathering of OM[7] because OM in the New Albany shale was only observed as blebs that were tens of micrometers in size.[17] Consistent with this, Wildman et al. reported almost 100% depletion of OM in the location of New Albany that they studied.[17] Therefore, the assumptions made by Bolton et al.[7] may be correct for that locality but not for the samples investigated in this study.

In contrast, microscopic observations shown here in Marcellus provide evidence of mineral-associated OM (Figures 2 and 9 and Figures S1 and S3 of the Supporting Information). Other researchers have reported profiles in New Albany and other shales that are incompletely developed, such as the profile described here (Figure 12). We hypothesize that OM in New Albany has different textural characteristics in different locations: in some locations, it is characterized only by large blebs of OM, and in others, it is characterized by large blebs and small disseminated particles. The mineral protection mechanism could also explain the greater depletion of OM during weathering of more clay-poor (carbonate-rich) shales, such as Green River, compared to clay-rich shales, such as Mancos and Pierre in the Colorado River Basin.[12,13,15,22]

Effect of the Erosion Rate. Oxidation of OM is expected to be more complete under landscapes with lower erosion rates because of longer residence times of rocks in the weathering zone and longer contact time with oxidizing fluids.[7] For eroding systems, completely developed profiles (100% depletion at the land surface) describe weathering where the rate of the reaction is fast compared to the rate of exposure of unaltered rock to surficial conditions of the rock by erosion. In contrast, incompletely developed profiles describe where the rate of delivery (erosion) is fast compared to weathering.

Equations predicting the extent of weathering of a phase as a function of the total denudation rate (=chemical dissolution + physical erosion) for systems that maintain a steady-state thickness of weathered material have been proposed.[77] Using three different rate constants k, we plotted identical curves based on the equations of Lebedeva et al.[77] along with observations from all 16 of the profiles published for

weathering sedimentary rock (mainly black shale) locations in Figure 12. Because the curves were calculated on the basis of a simple rock model consisting of albite plus quartz, they are not explicitly applicable to TOC and are only shown to emphasize how weathering might be expected to affect τ_{TOC} as a function of the erosion rate. Each profile was color-coded by the mean annual temperature (MAT), because we assumed that the kinetics of OM oxidation is positively correlated with MAT (k increases with increasing MAT).[78] Specifically, the figure shows three curves for arbitrary values of rate constants such that $k_1 < k_2 < k_3$. For most of the locations, no denudation rates are known; therefore, we grouped them assuming that values of the erosion rates were similar at basin scale. For example, the erosion rates of Appalachian Mountain shales (New Albany, labeled 1−3; Marcellus, labeled 4 and 5) are assumed to be within the range of 0.01−0.04 m kyear^{-1},[28] and the erosion rates of Colorado River Basin shales (Mancos, labeled 11 and 12; Pierre, labeled 13) are assumed to be within the range of 0.01−0.04 m kyear^{-1}.[79]

Some broad patterns of the plot show similarity to the model predictions. For example, the extent of depletion generally increases with MAT, and near-complete depletion ($\tau_{TOC} <$ −0.9) was only observed in the regions with lower erosion rates. In the regions with high erosion rate, on the contrary, the depletion of OC_{petro} is usually incomplete, even in some places with high MAT (e.g., Taiwan). Such incomplete profiles are consistent with the high amount of OC_{petro} observed in stream sediment in mountain belts where erosion rates are generally high.[80]

However, data from the regions with a low erosion rate are more scattered and cannot be explained entirely by differences in MAT (Figure 12). For example, within the Colorado River Basin, OM in Green River (labeled 7) is more depleted than that in Mancos (labeled 11 and 12) and Pierre (labeled 13). The Mancos shale from the East River watershed (Colorado, U.S.A., labeled 11) is more depleted than the same shale from Dry Wash Canyon (Utah, U.S.A., labeled 12) even though MAT at the former location is 8.5 °C lower. The complicated weathering patterns of OM indicate that factors in addition to the erosion rate and temperature must play a role in determining the extent of depletion of OM. As a result of the limited microscopic work in the published papers, we could not determine whether the factors are compositional (e.g., source and maturity of OM) or textural (particle size of OM). Furthermore, some profiles may have been measured at ridgetops and others near valley floors, and such different landscape positions are also expected to affect depletion profiles.[23,27] The differences in reactivity of larger blebs versus matrix-disseminated OM during shale weathering as observed in this work may suggests that future research should also target textural properties of the shale and its OM.

■ CONCLUSION

Oxidative weathering of OM in shale is an important process that contributes to controls of atmospheric CO_2 and O_2 over geologic time scales. In this study, we estimated the extent of OM depletion in saprock in an outcrop of Marcellus in central Pennsylvania, U.S.A. We found evidence of intensive weathering of carbonate, plagioclase, and pyrite in the saprock of Marcellus with little evidence of weathering in the underlying, carbonate-rich layer of the Onondaga Formation. Consistent with this, the porosities of saprock samples (20−24%) are more than 4 times higher than in the underlying Onondaga

Formation (~3.3%) or in the Marcellus bedrock (~5.8%) samples that were inferred to be a good indicator of parent rock. Decomposition of OM in the saprock leaves elongated pores in the size range from hundreds of nanometers to hundreds of micrometers and contributes to around $^2/_3$ of the weathering-generated porosity. Moreover, we found that the larger OM particles are preferentially decomposed during weathering, while the extent of depletion of smaller OM particles, which are usually associated with surfaces of aluminosilicate mineral grains, is much smaller. The best explanation for this is that OM is present in the shale as both large blebs and small disseminated clay-associated particles. The former oxidizes readily, while the latter is resistant to oxidation. Mineral protection and, to some extent, protection from possible microbial activity may explain the incompletely developed weathering profiles of OM in shales in regions with a low erosion rate. While the mechanism of mineral protection could be chemical in nature (a possibility not investigated here), the mechanism could also be related to the very small pore throats in the shale matrix that lower diffusivity and microbial access to the fine blebs but not the large blebs. A further study is needed to investigate not only how OM weathers but how the shale texture affects such weathering.

ASSOCIATED CONTENT

ⓢ Supporting Information

The Supporting Information is available free of charge at https://pubs.acs.org/doi/10.1021/acsearthspace-chem.1c00442.

> Additional BSE images and EDS results (Figures S1–S3), elemental concentrations of Marcellus shale samples from deep boreholes (Table S1), and summary of weathering profiles of OM in sedimentary rocks (Table S2) (PDF)

AUTHOR INFORMATION

Corresponding Author

Xin Gu − *Earth and Environmental Systems Institute and Department of Geosciences, The Pennsylvania State University, University Park, Pennsylvania 16802, United States; Environmental Sciences Division, Oak Ridge National Laboratory, Oak Ridge, Tennessee 37831, United States;* ⓞ orcid.org/0000-0003-3245-478X; Email: xug102@psu.edu

Author

Susan L. Brantley − *Earth and Environmental Systems Institute and Department of Geosciences, The Pennsylvania State University, University Park, Pennsylvania 16802, United States*

Complete contact information is available at:
https://pubs.acs.org/10.1021/acsearthspacechem.1c00442

Notes

The authors declare no competing financial interest.

ACKNOWLEDGMENTS

ABBREVIATIONS USED

BSE, backscattered electron; EDS, energy-dispersive X-ray spectroscopy; ICP−AES, inductively coupled plasma atomic emission spectroscopy; LOI, loss on ignition; MAT, mean annual temperature; mbls, meters below land surface; MIP, mercury intrusion porosimetry; NCNR, National Institute of Standards and Technology Center for Neutron Research; OC_{petro}, petrogenic organic carbon; OM, organic matter; PSD, pore size distribution; SANS, small-angle neutron scattering; SEM, scanning electron microscopy; SLD, scattering length density; TOC, total organic carbon; USANS, ultra-small-angle neutron scattering; XRD, X-ray diffraction

REFERENCES

(1) Berner, R. A.; Canfield, D. E. A New Model for Atmospheric Oxygen over Phanerozoic Time. *Am. J. Sci.* **1989**, *289* (4), 333−361.
(2) Torres, M. A.; West, A. J.; Li, G. J. Sulphide Oxidation and Carbonate Dissolution as a Source of CO_2 over Geological Timescales. *Nature* **2014**, *507* (7492), 346−349.
(3) Kump, L. R.; Brantley, S. L.; Arthur, M. A. Chemical Weathering, Atmospheric CO_2, and Climate. *Annu. Rev. Earth Planet. Sci.* **2000**, *28* (1), 611−667.
(4) Brantley, S. L.; Lebedeva, M.; Bazilevskaya, E. Relating Weathering Fronts for Acid Neutralization and Oxidation to pCO_2 and pO_2. In *Treatise on Geochemistry*, 2nd ed.; Elsevier: Amsterdam, 2014; Vol. *6*, Chapter 6.15, pp 327−352. DOI: 10.1016/B978-0-08-095975-7.01317-6.
(5) Hilton, R. G.; West, A. J. Mountains, Erosion and the Carbon Cycle. *Nat. Rev. Earth Environ.* **2020**, *1* (6), 284−299.

(6) Maffre, P.; Swanson-Hysell, N. L.; Goddéris, Y. Limited Carbon Cycle Response to Increased Sulfide Weathering Due to Oxygen Feedback. *Geophys. Res. Lett.* **2021**, *48* (19), e2021GL094589.

(7) Bolton, E. W.; Berner, R. A.; Petsch, S. T. The Weathering of Sedimentary Organic Matter as a Control on Atmospheric O_2: II. Theoretical Modeling. *Am. J. Sci.* **2006**, *306* (8), 575−615.

(8) Petsch, S. T. Weathering of Organic Carbon. In *Treatise on Geochemistry*, 2nd ed.; Elsevier: Amsterdam, 2014; Vol. 12, Chapter 12.8, pp 217−238. DOI: 10.1016/B978-0-08-095975-7.01013-5.

(9) Amiotte Suchet, P.; Probst, J.-L.; Ludwig, W. Worldwide Distribution of Continental Rock Lithology: Implications for the Atmospheric/soil CO_2 Uptake by Continental Weathering and Alkalinity River Transport to the Oceans. *Global Biogeochem. Cycles* **2003**, *17* (2), 1038.

(10) Hartmann, J.; Moosdorf, N. The New Global Lithological Map Database GLiM: A Representation of Rock Properties at the Earth Surface. *Geochem., Geophys., Geosyst.* **2012**, *13* (12), Q12004.

(11) Copard, Y.; Amiotte-Suchet, P.; Di-Giovanni, C. Storage and Release of Fossil Organic Carbon Related to Weathering of Sedimentary Rocks. *Earth Planet. Sci. Lett.* **2007**, *258* (1−2), 345−357.

(12) Leythaeuser, D. Effects of Weathering on Organic-matter in Shales. *Geochim. Cosmochim. Acta* **1973**, *37*, 113−120.

(13) Clayton, J. L.; Swetland, P. J. Subaerial weathering of sedimentary organic matter. *Geochim. Cosmochim. Acta* **1978**, *42*, 305−312.

(14) Littke, R.; Klussmann, U.; Krooss, B.; Leythaeuser, D. Quantification of Loss of Calcite, Pyrite, and Organic Matter Due to Weathering of Toarcian Black Shales and Effects on Kerogen and Bitumen Characteristics. *Geochim. Cosmochim. Acta* **1991**, *55* (11), 3369−3378.

(15) Petsch, S. T.; Berner, R. A.; Eglinton, T. I. A Field Study of the Chemical Weathering of Ancient Sedimentary Organic Matter. *Org. Geochem.* **2000**, *31* (5), 475−487.

(16) Jaffe, L. A.; Peucker-Ehrenbrink, B.; Petsch, S. T. Mobility of Rhenium, Platinum Group Elements and Organic Carbon During Black Shale Weathering. *Earth Planet. Sci. Lett.* **2002**, *198* (3−4), 339−353.

(17) Wildman, R. A.; Berner, R. A.; Petsch, S. T.; Bolton, E. W.; Eckert, J. O.; Mok, U.; Evans, J. B. The Weathering of Sedimentary Organic Matter as a Control on Atmospheric O_2: I. Analysis of a Black Shale. *Am. J. Sci.* **2004**, *304* (3), 234−249.

(18) Fischer, C.; Gaupp, R. Change of Black Shale Organic Material Surface Area During Oxidative Weathering: Implications for Rock-Water Surface Evolution. *Geochim. Cosmochim. Acta* **2005**, *69* (5), 1213−1224.

(19) Tuttle, M. L. W.; Breit, G. N. Weathering of the New Albany Shale, Kentucky, USA: I. Weathering Zones Defined by Mineralogy and Major-Element Composition. *Appl. Geochem.* **2009**, *24* (8), 1549−1564.

(20) Jin, L. X.; Mathur, R.; Rother, G.; Cole, D.; Bazilevskaya, E.; Williams, J.; Carone, A.; Brantley, S. Evolution of Porosity and Geochemistry in Marcellus Formation Black Shale During Weathering. *Chem. Geol.* **2013**, *356*, 50−63.

(21) Tuttle, M. L. W.; Fahy, J. W.; Elliott, J. G.; Grauch, R. I.; Stillings, L. L. Contaminants from Cretaceous Black Shale: I. Natural Weathering Processes Controlling Contaminant Cycling in Mancos Shale, Southwestern United States, with Emphasis on Salinity and Selenium. *Appl. Geochem.* **2014**, *46*, 57−71.

(22) Wan, J.; Tokunaga, T. K.; Williams, K. H.; Dong, W.; Brown, W.; Henderson, A. N.; Newman, A. W.; Hubbard, S. S. Predicting Sedimentary Bedrock Subsurface Weathering Fronts and Weathering Rates. *Sci. Rep.* **2019**, *9* (1), 17198.

(23) Pedrazas, M. A.; Hahm, W. J.; Huang, M.-H.; Dralle, D.; Nelson, M. D.; Breunig, R. E.; Fauria, K. E.; Bryk, A. B.; Dietrich, W. E.; Rempe, D. M. The Relationship Between Topography, Bedrock Weathering, and Water Storage Across a Sequence of Ridges and Valleys. *J. Geophys. Res.: Earth Surf.* **2021**, *126* (4), e2020JF005848.

(24) Brantley, S. L.; Lebedeva, M. Learning to Read the Chemistry of Regolith to Understand the Critical Zone. *Annu. Rev. Earth Planet. Sci.* **2011**, *39*, 387−416.

(25) Gu, X.; Heaney, P. J.; Reis, F. D. A. A.; Brantley, S. L. Deep Abiotic Weathering of Pyrite. *Science* **2020**, *370* (6515), eabb8092.

(26) Lasaga, A. C.; Ohmoto, H. The Oxygen Geochemical Cycle: Dynamics and Stability. *Geochim. Cosmochim. Acta* **2002**, *66* (3), 361−381.

(27) Gu, X.; Rempe, D. M.; Dietrich, W. E.; West, A. J.; Lin, T.-C.; Jin, L.; Brantley, S. L. Chemical Reactions, Porosity, and Micro-fracturing in Shale During Weathering: The Effect of Erosion Rate. *Geochim. Cosmochim. Acta* **2020**, *269*, 63−100.

(28) Miller, S. R.; Sak, P. B.; Kirby, E.; Bierman, P. R. Neogene Rejuvenation of Central Appalachian Topography: Evidence for Differential Rock Uplift from Stream Profiles and Erosion Rates. *Earth Planet. Sci. Lett.* **2013**, *369−370*, 1−12.

(29) Heidari, P.; Li, L.; Jin, L.; Williams, J. Z.; Brantley, S. L. A Reactive Transport Model for Marcellus Shale Weathering. *Geochim. Cosmochim. Acta* **2017**, *217*, 421−440.

(30) Petsch, S. T.; Smernik, R. J.; Eglinton, T. I.; Oades, J. M. A Solid State ^{13}C-NMR Study of Kerogen Degradation During Black Shale Weathering. *Geochim. Cosmochim. Acta* **2001**, *65*, 1867−1882.

(31) Kohl, D.; Slingerland, R.; Arthur, M.; Bracht, R.; Engelder, T. Sequence Stratigraphy and Depositional Environments of the Shamokin (Union Springs) Member, Marcellus Formation, and Associated Strata in the Middle Appalachian Basin. *AAPG Bull.* **2014**, *98* (3), 483−513.

(32) Mathur, R.; Jin, L.; Prush, V.; Paul, J.; Ebersole, C.; Fornadel, A.; Williams, J. Z.; Brantley, S. Cu Isotopes and Concentrations During Weathering of Black Shale of the Marcellus Formation, Huntingdon County, Pennsylvania (USA). *Chem. Geol.* **2012**, *304−305*, 175−184.

(33) Brantley, S. L.; White, T.; West, N.; Williams, J. Z.; Forsythe, B.; Shapich, D.; Kaye, J.; Lin, H.; Shi, Y.; Kaye, M.; Herndon, E.; Davis, K. J.; He, Y.; Eissenstat, D.; Weitzman, J.; DiBiase, R.; Li, L.; Reed, W.; Brubaker, K.; Gu, X. Susquehanna Shale Hills Critical Zone Observatory: Shale Hills in the Context of Shaver's Creek Watershed. *Vadose Zone J.* **2018**, *17* (1), 1−19.

(34) Engelder, T.; Slingerland, R.; Arthur, M.; Lash, G.; Kohl, D.; Gold, D. P.; Ruffolo, R. M.; Ciampaglio, C. N. An Introduction to Structures and Stratigraphy in the Proximal Portion of the Middle Devonian Marcellus and Burket/Geneseo Black Shales in the Central Appalachian Valley and Ridge. In *From the Shield to the Sea*; GSA Field Guide, Vol. 20; Geological Society of America: Boulder, CO, 2011; pp 17−44. DOI: 10.1130/2011.0020(02).

(35) Gu, X.; Cole, D. R.; Rother, G.; Mildner, D. F. R.; Brantley, S. L. Pores in Marcellus Shale: A Neutron Scattering and FIB-SEM Study. *Energy Fuels* **2015**, *29* (3), 1295−1308.

(36) Gu, X.; Mildner, D. F. R.; Cole, D. R.; Rother, G.; Slingerland, R.; Brantley, S. L. Quantification of Organic Porosity and Water Accessibility in Marcellus Shale Using Neutron Scattering. *Energy Fuels* **2016**, *30* (6), 4438−4449.

(37) Brimhall, G. H.; Dietrich, W. E. Constitutive Mass Balance Relations Between Chemical-Composition, Volume, Density, Poros-ity, and Strain in Metasomatic Hydrochemical Systems: Results on Weathering and Pedogenesis. *Geochim. Cosmochim. Acta* **1987**, *51* (3), 567−587.

(38) Anderson, S. P.; Dietrich, W. E.; Brimhall, G. H. Weathering Profiles, Mass-Balance Analysis, and Rates of Solute Loss: Linkages Between Weathering and Erosion in a Small, Steep Catchment. *Geol. Soc. Am. Bull.* **2002**, *114* (9), 1143−1158.

(39) Kim, H.; Gu, X.; Brantley, S. L. Particle Fluxes in Groundwater Change Subsurface Shale Rock Chemistry over Geologic Time. *Earth Planet. Sci. Lett.* **2018**, *500*, 180−191.

(40) Eberl, D. D. *User's Guide to RockJock—A Program for Determining Quantitative Mineralogy from Powder X-ray Diffraction Data*; United States Geological Survey: Reston, VA, 2003; Open-File Report 2003-78.

(41) Abramoff, M. D.; Magalhães, P. J.; Ram, S. J. Image Processing with ImageJ. *Biophotonics Int.* **2004**, *11*, 36−42.

(42) Thompson, A. H.; Katz, A. J.; Krohn, C. E. The Microgeometry and Transport Properties of Sedimentary Rock. *Adv. Phys.* **1987**, *36* (5), 625−694.

(43) Radlinski, A. P. Small-Angle Neutron Scattering and the Microstructure of Rocks. *Rev. Mineral. Geochem.* **2006**, *63*, 363−397.

(44) Anovitz, L. M.; Cole, D. R. Characterization and Analysis of Porosity and Pore Structures. *Rev. Mineral. Geochem.* **2015**, *80*, 61−164.

(45) Glinka, C. J.; Barker, J. G.; Hammouda, B.; Krueger, S.; Moyer, J. J.; Orts, W. J. The 30 M Small-Angle Neutron Scattering Instruments at the National Institute of Standards and Technology. *J. Appl. Crystallogr.* **1998**, *31* (3), 430−445.

(46) Barker, J. G.; Glinka, C. J.; Moyer, J. J.; Kim, M. H.; Drews, A. R.; Agamalian, M. Design and Performance of a Thermal-Neutron Double-Crystal Diffractometer for USANS at NIST. *J. Appl. Crystallogr.* **2005**, *38* (6), 1004−1011.

(47) Page, S. A.; Berg, J. C.; Månson, J.-A. E. Characterization of Epoxy Resin Surface Energetics. *J. Adhes. Sci. Technol.* **2001**, *15*, 153−170.

(48) van de Grampel, R. D.; Ming, W.; van Gennip, W. J. H.; van der Velden, F.; Laven, J.; Niemantsverdriet, J. W.; van der Linde, R. Thermally Cured Low Surface-Tension Epoxy Films. *Polymer* **2005**, *46*, 10531−10537.

(49) Shah, S. M.; Crawshaw, J. P.; Boek, E. S. Preparation of Microporous Rock Samples for Confocal Laser Scanning Microscopy. *Pet. Geosci.* **2014**, *20*, 369−374.

(50) Balashov, V. N.; Engelder, T.; Gu, X.; Fantle, M. S.; Brantley, S. L. A Model Describing Flowback Chemistry Changes with Time After Marcellus Shale Hydraulic Fracturing. *AAPG Bull.* **2015**, *99* (1), 143−154.

(51) Kline, S. R. Reduction and Analysis of SANS and USANS Data Using IGOR Pro. *J. Appl. Crystallogr.* **2006**, *39* (6), 895−900.

(52) Anovitz, L. M.; Cole, D. R.; Rother, G.; Allard, L. F.; Jackson, A. J.; Littrell, K. C. Diagenetic Changes in Macro- to Nano-Scale Porosity in the St. Peter Sandstone: An (Ultra) Small Angle Neutron Scattering and Backscattered Electron Imaging Analysis. *Geochim. Cosmochim. Acta* **2013**, *102*, 280−305.

(53) Hinde, A. L. PRINSAS—A Windows-Based Computer Program for the Processing and Interpretation of Small-Angle Scattering Data Tailored to the Analysis of Sedimentary Rocks. *J. Appl. Crystallogr.* **2004**, *37*, 1020−1024.

(54) Clark, S. H.; Mosier, E. L. *Barite Nodules in Devonian Shale and Mudstone of Western Virginia*; United States Geological Survey: Reston, VA, 1989; Bulletin 1880.

(55) Wang, J.; Arthur, M. A. The Diagenetic Origin and Depositional History of the Cherry Valley Member, Middle Devonian Marcellus Formation. *Chem. Geol.* **2020**, *558*, 119875.

(56) Hosterman, J. W.; Whitlow, S. I. *Clay Mineralogy of Devonian Shales in the Appalachian Basin*; United States Geological Survey: Reston, VA, 1983; Professional Paper 1298.

(57) Wang, G. C.; Carr, T. R. Marcellus Shale Lithofacies Prediction by Multiclass Neural Network Classification in the Appalachian Basin. *Math. Geosci.* **2012**, *44* (8), 975−1004.

(58) Chigira, M.; Oyama, T. Mechanism and Effect of Chemical Weathering of Sedimentary Rocks. *Eng. Geol.* **2000**, *55* (1−2), 3−14.

(59) Brantley, S. L.; Holleran, M. E.; Jin, L. X.; Bazilevskaya, E. Probing Deep Weathering in the Shale Hills Critical Zone Observatory, Pennsylvania (USA): The Hypothesis of Nested Chemical Reaction Fronts in the Subsurface. *Earth Surf. Processes Landforms* **2013**, *38* (11), 1280−1298.

(60) Hochella, M. F.; Moore, J. N.; Golla, U.; Putnis, A. A TEM Study of Samples from Acid Mine Drainage Systems: Metal-Mineral Association with Implications for Transport. *Geochim. Cosmochim. Acta* **1999**, *63* (19), 3395−3406.

(61) Dutrizac, J. E.; Jambor, J. L. Jarosites and Their Application in Hydrometallurgy. *Rev. Mineral. Geochem.* **2000**, *40* (1), 405−452.

(62) Madden, M. E. E.; Madden, A. S.; Rimstidt, J. D.; Zahrai, S.; Kendall, M. R.; Miller, M. A. Jarosite Dissolution Rates and Nanoscale Mineralogy. *Geochim. Cosmochim. Acta* **2012**, *91*, 306−321.

(63) Hemingway, J. D.; Hilton, R. G.; Hovius, N.; Eglinton, T. I.; Haghipour, N.; Wacker, L.; Chen, M. C.; Galy, V. V. Microbial Oxidation of Lithospheric Organic Carbon in Rapidly Eroding Tropical Mountain Soils. *Science* **2018**, *360* (6385), 209−212.

(64) Brantley, S. L.; White, A. F. Approaches to Modeling Weathered Regolith. *Rev. Mineral. Geochem.* **2009**, *70*, 435−484.

(65) Loucks, R. G.; Reed, R. M. Scanning-Electron-Microscope Petrographic Evidence for Distinguishing Organic-Matter Pores Associated with Depositional Organic Matter Versus Migrated Organic Matter in Mudrocks. *GCAGS J.* **2014**, *3*, 51−60.

(66) Hemingway, J. D.; Rothman, D. H.; Grant, K. E.; Rosengard, S. Z.; Eglinton, T. I.; Derry, L. A.; Galy, V. V. Mineral Protection Regulates Long-Term Global Preservation of Natural Organic Carbon. *Nature* **2019**, *570* (7760), 228−231.

(67) Hasenmueller, E. A.; Gu, X.; Weitzman, J. N.; Adams, T. S.; Stinchcomb, G. E.; Eissenstat, D. M.; Drohan, P. J.; Brantley, S. L.; Kaye, J. P. Weathering of Rock to Regolith: The Activity of Deep Roots in Bedrock Fractures. *Geoderma* **2017**, *300*, 11−31.

(68) Hull, K. L.; Jacobi, D.; Abousleiman, Y. N. Oxidative Kerogen Degradation: A Potential Approach to Hydraulic Fracturing in Unconventionals. *Energy Fuels* **2019**, *33*, 4758−4766.

(69) Petsch, S. T.; Eglinton, T. I.; Edwards, K. J. ^{14}C-Dead Living Biomass: Evidence for Microbial Assimilation of Ancient Organic Carbon During Shale Weathering. *Science* **2001**, *292* (5519), 1127−1131.

(70) Wengel, M.; Kothe, E.; Schmidt, C. M.; Heide, K.; Gleixner, G. Degradation of Organic Matter from Black Shales and Charcoal by the Wood-Rotting Fungus *Schizophyllum commune* and Release of DOC and Heavy Metals in the Aqueous Phase. *Sci. Total Environ.* **2006**, *367*, 383−393.

(71) Luef, B.; Frischkorn, K. R.; Wrighton, K. C.; Holman, H.-Y. N.; Birarda, G.; Thomas, B. C.; Singh, A.; Williams, K. H.; Siegerist, C. E.; Tringe, S. G.; Downing, K. H.; Comolli, L. R.; Banfield, J. F. Diverse Uncultivated Ultra-Small Bacterial Cells in Groundwater. *Nat. Commun.* **2015**, *6*, 6372.

(72) Mayer, L. M.; Schick, L. L.; Hardy, K. R.; Wagai, R.; McCarthy, J. Organic Matter in Small Mesopores in Sediments and Soils. *Geochim. Cosmochim. Acta* **2004**, *68* (19), 3863−3872.

(73) McCarthy, J. F.; Ilavsky, J.; Jastrow, J. D.; Mayer, L. M.; Perfect, E.; Zhuang, J. Protection of Organic Carbon in Soil Microaggregates via Restructuring of Aggregate Porosity and Filling of Pores with Accumulating Organic Matter. *Geochim. Cosmochim. Acta* **2008**, *72* (19), 4725−4744.

(74) Kennedy, M. J.; Pevear, D. R.; Hill, R. J. Mineral Surface Control of Organic Carbon in Black Shale. *Science* **2002**, *295* (5555), 657−660.

(75) Mayer, L. M. Relationships Between Mineral Surfaces and Organic Carbon Concentrations in Soils and Sediments. *Chem. Geol.* **1994**, *114* (3), 347−363.

(76) Ransom, B.; Kim, D.; Kastner, M.; Wainwright, S. Organic Matter Preservation on Continental Slopes: Importance of Mineralogy and Surface Area. *Geochim. Cosmochim. Acta* **1998**, *62* (8), 1329−1345.

(77) Lebedeva, M. I.; Fletcher, R. C.; Brantley, S. L. A Mathematical Model for Steady-State Regolith Production at Constant Erosion Rate. *Earth Surf. Processes Landforms* **2010**, *35* (5), 508−524.

(78) Soulet, G.; Hilton, R. G.; Garnett, M. H.; Roylands, T.; Klotz, S.; Croissant, T.; Dellinger, M.; Le Bouteiller, C. Temperature Control on CO_2 Emissions from the Weathering of Sedimentary Rocks. *Nat. Geosci.* **2021**, *14*, 665−671.

(79) Dethier, D. P.; Ouimet, W.; Bierman, P. R.; Rood, D. H.; Balco, G. Basins and Bedrock: Spatial Variation in [10]Be Erosion Rates and Increasing Relief in the Southern Rocky Mountains, USA. *Geology* **2014**, *42* (2), 167−170.

(80) Hilton, R. G.; Galy, A.; Hovius, N.; Horng, M. J.; Chen, H. Efficient Transport of Fossil Organic Carbon to the Ocean by Steep

Mountain Rivers: An Orogenic Carbon Sequestration Mechanism. *Geology* **2011**, *39*, 71−74.